PHYSICAL REVIEW B **75**, 161303(R) (2007)

Elastic strain relaxation in axial Si/Ge whisker heterostructures

M. Hanke and C. Eisenschmidt
Martin-Luther-Universität Halle-Wittenberg, Institut für Physik, Hoher Weg 8, D-06120 Halle/Saale, Germany

P. Werner and N. D. Zakharov
Max-Planck Institut für Mikrostrukturphysik, Weinberg 2, D-06120 Halle/Saale, Germany

F. Syrowatka and F. Heyroth
Interdisziplinäres Zentrum für Materialwissenschaften, Heinrich-Damerow-Straße 4, D-06120 Halle/Saale

P. Schäfer
Humboldt-Universität zu Berlin, Institut für Physik, Newtonstraße 15, D-12489 Berlin, Germany

O. Konovalov
European Synchrotron Radiation Facility, BP 220, F-38043 Grenoble Cedex, France
(Received 14 March 2007; revised manuscript received 11 April 2007; published 23 April 2007)

The elastic behavior of molecular beam epitaxy–grown SiGe/Si(111) nanowhiskers (NWs) has been studied by means of electron microscopy, x-ray scattering, and numerical linear elasticity theory. Highly brilliant synchrotron radiation was applied to map the diffusely scattered intensity near the asymmetric (115) reciprocal lattice point. The larger lattice parameter with respect to the Si matrix causes a lateral lattice expansion within embedded Ge layers. This enables a clear separation of scattering due to NWs and laterally confined areas aside. Finite element calculations prove a lateral lattice compression in the Si matrix close to the NW apex above buried threefold and single Ge layer stacks. This suggests an incorporation probability, which additionally depends on the radial position within heteroepitaxial NWs.

DOI: 10.1103/PhysRevB.75.161303 PACS number(s): 68.70.+w, 61.10.Nz, 68.37.Lp

One-dimensional semiconductor structures, also referred to as nanowires and nanowhiskers (NWs), have attracted much interest during recent years due to their manyfold potential applications in electronics, photonics, and sensing devices, for example.[1,2] So, at first glance it may be surprising that the homoepitaxial growth of Si whiskers via the vapor-liquid solid (VLS) mechanism was already explored nearly 40 years ago,[3] however, only on a μm scale. Silicon NWs can be successfully grown by applying the VLS process. In the case of the mainly used chemical vapor deposition technique, a Si containing gas/precursor is cracked at Au droplets acting as seeds. Si adatoms are subsequently solved in the liquid metal. Due to a supersaturation within this droplet, Si precipitates predominantly at the liquid-solid interface and a nanowhisker appears. A somewhat completely different situation occurs if NWs are grown by molecular beam epitaxy (MBE) via the VLS mechanism as applied in the present experiments. This concerns, e.g., the role of the metal seed, the morphology of the NWs, and the aspect ratio of their lengths and widths. Surface diffusion especially, including the metal used as well as Si, strongly influences the growth process. More recently, various groups have demonstrated Si NWs on Si,[4,5] Ge NWs on Si,[6] axial heterostructures by embedding Ge layers into Si NWs,[7,8] as well as radial core-shell Si/Ge NWs.[9] The mutual impact of the chemical composition, the established elastic strain and its eventual relaxation influences the further growth sequence regardless of the particular structure or growth method. Regarding characterization, most groups, however, still rely on direct imaging techniques such as electron microscopy, whereas x-ray scattering techniques very recently emerge in the NW field.[1] In this paper, we applied electron microscopy, diffuse x-ray scattering, and numerical finite element method (FEM) to probe composition, strain, and elastic relaxation within heteroepitaxial Si/Ge NWs.

The samples have been grown on ⟨111⟩-oriented five inch Si wafers, which were cleaned by conventional RCA procedure. Our MBE system includes three electron-beam guns for the evaporation of Au and Si as well as of Ge.[7] A thin Au film with a nominal thickness of 2 nm was deposited on the substrate at a substrate temperature T_S of 525 °C forming small gold droplets. During the following NW growth, the constant Si and Ge fluxes amounted to 0.05 and 0.01 nm/s, respectively. Since in the vapor-liquid-solid mechanism the gold droplets act as the intermediate and hence liquid medium, they will not induce additional strain into the NWs.

Both the chemical profile and the closely related strain distribution within the NWs determine mechanical and optical properties of the NWs. Thus, to probe the three-dimensional strain profile we have employed high resolution x-ray diffraction (HRXRD). Respective experiments were performed at the beamline ID10B at the European Synchrotron Radiation Facility (ESRF) using an x-ray energy of 7951 eV. In the actual setup we applied a positional sensitive detector (PSD) with a nominal pixel size of 60 μm corresponding to a resolution of 0.004 Å^{-1}. An additional 1 mm slit in front of the PSD restricts the resolution perpendicular to the scattering plane to about 0.006 Å^{-1}.

Figure 1 shows reciprocal space maps of the diffuse intensity near the asymmetric (115) reflection for the three samples depicted in Fig. 2: pure Si NWs (a), NWs containing a single Ge disk (b), and a threefold vertical stack (c). In the

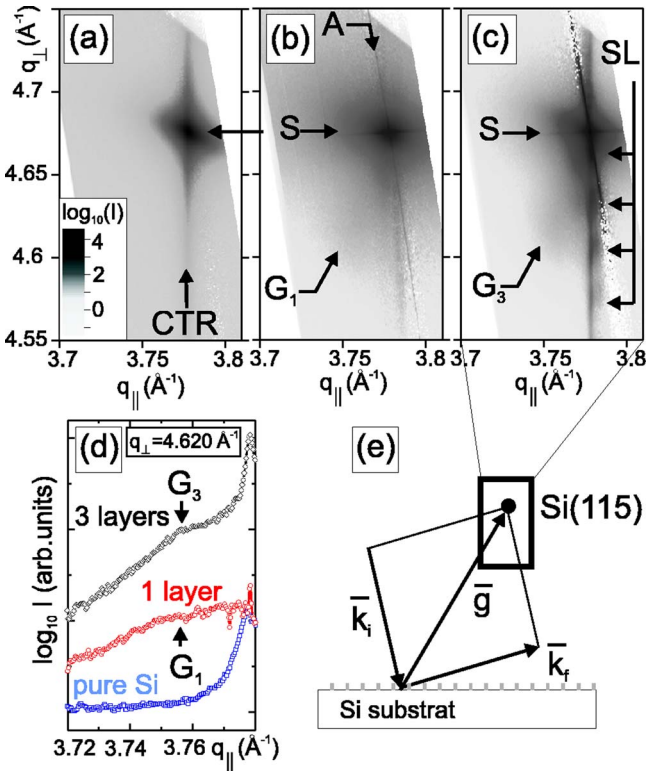

FIG. 1. (Color online) Diffusely scattered intensity near the asymmetric Si(115) reflection (S) for samples with pure Si NWs (a), those containing a single Ge layer (b), and three layers (c), respectively. Since pattern (a) only reveals diffuse intensity near the substrate reflection (S), the further distributions (b) and (c) probe laterally relaxed lattice sites (G_1 and G_3). Due to the vertical superstructure in the threefold system, additional intensity oscillations (SL) become prominent along the crystal truncation rod (CTR) in (c). (d) shows line scans through the reciprocal space maps (a)–(c) at $q_\perp = 4.620$ Å^{-1} for a quantitative estimate of the positions G_1 and G_3. Scheme (e) illustrates how the diffraction vector $\bar{g}$ may probe diffuse intensity in reciprocal space by varying the directions of the incident and exit wave vectors, $\bar{k}_i$ and $\bar{k}_f$.

limit of pure Si, no elastic strain is anticipated in the structure. In such an ideal limit there are, hence, no deformed lattice sites, which may cause additional diffuse scattering. However, as soon as a heteroepitaxial layer is embedded within the NWs, the various lattice constants will induce strain energy. During the further NW growth it may be lowered because a one-dimensional structure provides excellent conditions to elastically relax perpendicular to its axial direction. The transmission electron micrographs (TEM) in Figs. 2(b)–2(d) indicate that this favorably happens elastically, thus without the formation of misfit dislocations.

The scattering vector q_{115} displays nearly equivalent, nonzero lateral, $q_\parallel^{Si} = 3.778$ Å^{-1}, and vertical, $q_\perp^{Si} = 4.674$ Å^{-1}, components. Thus, it probes the normalized lattice constant parallel $(\Delta a/a)_\parallel$ and perpendicular $(\Delta a/a)_\perp$ to the mean surface with similar sensitivity. Consequently, sample areas, which may laterally relax, imply diffuse intensity well separated from contributions due to laterally confined regions. This enables in particular a clear distinction between scattering due to NWs and the adjacent planar structure. Scattering

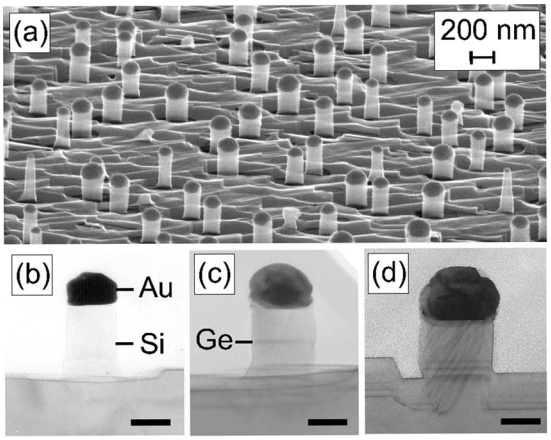

FIG. 2. Scanning electron micrograph of a sample containing pure Si NWs (a). (b) to (d): TEM micrographs of individual NWs of pure Si, NWs with an embedded single Ge layer and with three layers, respectively. The bar corresponds to 100 nm.

on nonstrained, pure Si NWs accordingly cause only an intense Si(115) reflection (*S*), Fig. 1(a). Additional intensive spots G_1 and G_3 in Fig. 1(b) and 1(c) serve as fingerprints to strain and composition of the embedded heteroepitaxial layers. The scattered intensity cloud around G_1 in Fig. 1(b) is caused by a single layer and appears comparatively weak at about $q_\parallel = 3.759$ Å^{-1}, $q_\perp = 4.620$ Å^{-1}. The larger extension of peak G_1 (compared with G_3) refers to a broader size distribution of the NW radii, which is about ±10% for the single and ±5% for the three layers sample. However, for the threefold embedded Ge structure, the feature becomes more intense, whereas its position does not change significantly. Moreover, the presence of a (115) reflection clearly indicates zinc-blende stacking along the [111] axis. The lateral and vertical lattice deformations $(\Delta a/a)_{\parallel,\perp}$ directly correspond to respective peak positions in reciprocal space $(\Delta q/q)_{\parallel,\perp}$, which eventually yields a relaxed lattice mismatch:

$$(\Delta a/a)_{\mathrm{rel}} = P_{111}[(\Delta a/a)_\perp - (\Delta a/a)_\parallel] + (\Delta a/a)_\parallel. \quad (1)$$

Here we consider the orientation dependent factor P_{111}:[10,11]

$$P_{111} = \frac{C_{11} + \frac{2}{3}(2C_{44} - C_{11} + C_{12})}{C_{11} + 2C_{12}}. \quad (2)$$

Close positions of peak G_1 and G_3, Fig. 1(d), and hence a similar value for $(\Delta a/a)_{\mathrm{rel}} = 0.010$, indicate about 24% Ge within the heterostructure—independent of the particular number of layers. Further on, the relaxation parameter $R = (\Delta a/a)_\parallel / (\Delta a/a)_{\mathrm{rel}}$ gives the degree to which the lattice has been relaxed. It yields 0.0 for an ideal pseudomorphically strained layer, 1.0 for fully relaxed layers, and about 0.51 for the structures investigated here. A similar value for both structures indicates that the threefold layers (compared with the single layer) do not increase the degree of relaxation, whereas the amount of material in a certain strain status naturally increases for the threefold system. In other words: there is no cumulative strain effect. Each Ge layer acts independent from each other in terms of relaxation.

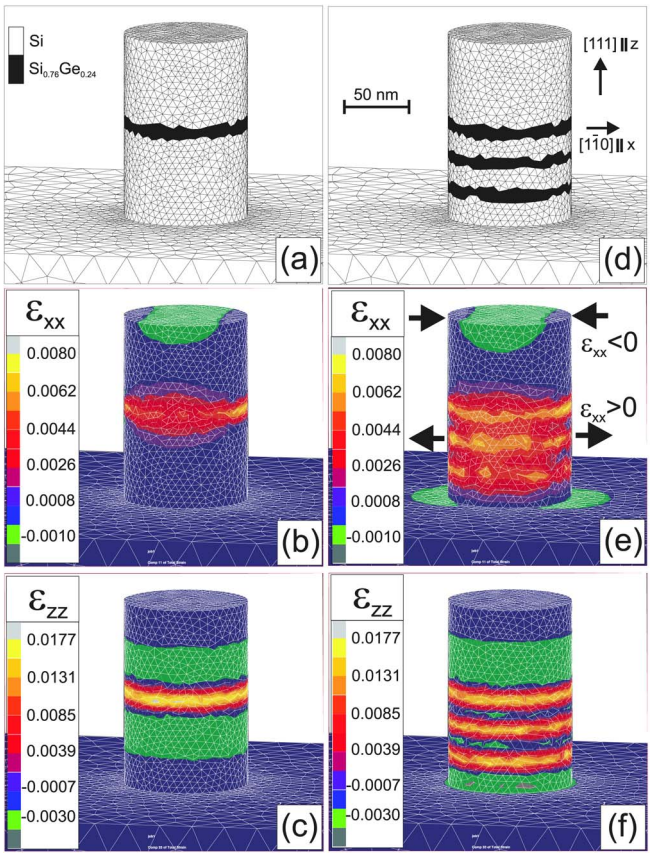

FIG. 3. (Color online) Model structures used for the FEM simulations and their results. Lateral (b),(e) and vertical (c),(f) total strain tensor components, ϵ_{xx} and ϵ_{zz}, as numerically revealed by finite element calculations. The models consider a single Ge layer (a) and a threefold vertical structure (d), respectively according to the micrographs, as shown in Fig. 2.

Considering the Ge content revealed by HRXRD, we have simulated the relaxation behavior within the NWs. In this regard, finite element calculations serve as a well-established analytical tool to calculate strain and relaxation in low-dimensional structures on the base of linear elasticity theory. (See, for example, Refs. 12 and 13). Both models displayed in Fig. 3(a) and 3(c) outline a single cylindrical NW according to the mean dimensions as revealed by electron microscopy (radius 50 nm, height 150 nm). The NWs are placed on a Si(111) substrate with lateral dimensions of $200\times200\times200$ nm^3, which sufficiently ensure a realistic elastic interaction. Since the first model (a) considers a single 10 nm $Si_{0.76}Ge_{0.24}$ disk embedded in the center, the further one (d) regards three subsequent layers (10 nm) vertically separated by 15 nm silicon spacers. The resulting lateral and vertical components of the total strain tensor, ϵ_{xx} and ϵ_{zz}, are plotted in Fig. 3(b), 3(c), 3(e), and 3(f). Obviously the larger Ge lattice causes either for single or multifold layers a vertical lattice expansion ($\epsilon_{zz}>0$) within the disks, whereas adjacent regions within the Si matrix undergo a compression ($\epsilon_{zz}<0$), which becomes in particular prominent for the single layer. An embedded multilayer structure yields, on the other hand, vertically well separated areas of lateral expansion ($\epsilon_{xx}>0$) marked by arrows in Fig. 3(e). However, it turns into negative values of about −0.1% at the NW apex Fig. 3(b) and 3(e), which indicates laterally compressed lattice sites, in particular close to the NW axis. This result proves a radial dependence of the lateral lattice parameter at the growth front above buried heteroepitaxial Ge layers, and hence suggests different incorporation probabilities at various radii. Moreover, it strongly supports the observation that Ge can be incorporated in axial Si/Ge NWs only in a Si-rich alloy up to about 25% Ge.[14]

The elastic strain and its relaxation in a set of MBE-grown Si/Ge NWs on Si(111) have been studied by means of electron microscopy, high resolution x-ray diffraction, and numerical finite element method. The samples contain either pure Si NWs, NWs with an embedded single SiGe layer, or a threefold stack of SiGe layers. The quasi-one-dimensional morphology of NWs sufficiently provides elastic relief perpendicular to the axial direction, which is proved by finite element calculations. Different degrees of lateral relaxation within NWs and adjacent laterally confined areas enable a clear distinction between respective contributions to the intensity pattern around the asymmetrical (115) reflection. Finite element calculations indicate moreover a laterally compressed Si matrix above buried Ge layers, which can be attributed to the stiffness of the NW lattice. Since this effect depends on the radial position at the NW apex, it suggests a radial dependent incorporation probability in vertically structured NWs.

We acknowledge financial support by the Federal State of Sachsen-Anhalt, Germany, within the Cluster of Excellence (CoE) *Nanostructured Materials*, Project Nos. NW2 (P.W.) and NW3 (M.H.), and Project No. NODE 015783. The authors thank the ESRF for providing beamtime during experiment HS-2652.

[1] C. P. T. Svenson, W. Seifert, M. W. Larsson, L. R. Wallenberg, J. Stangl, G. Bauer, and L. Samuelson, Nanotechnology **16**, 936 (2005).
[2] H. J. Fan, P. Werner, and M. Zacharias, Small **2**, 700 (2006).
[3] R. S. Wagner, *Whisker Technology* (Wiley, New York, 1970).
[4] T. I. Kamins, R. S. Williams, D. P. Basile, T. Hesjedal, and J. S. Harris, J. Appl. Phys. **89**, 1008 (2001).
[5] N. Ozaki, Y. Ohno, and S. Takeda, Appl. Phys. Lett. **73**, 3700 (1998).
[6] T. I. Kamins, X. Li, and R. S. Williams, Nano Lett. **4**, 503 (2004).
[7] L. Schubert, P. Werner, N. D. Zakharov, G. Gerth, F. Kolb, L. Long, U. Gösele, and T. Y. Tan, Appl. Phys. Lett. **84**, 4968 (2004).
[8] Y. Wu, R. Fan, and P. Yang, Nano Lett. **2**, 83 (2002).
[9] L. J. Lauhon, M. S. Gudikson, D. Wang, and C. M. Lieber, Nature (London) **420**, 57 (2002).

[10] J. Hornstra and W. J. Bartels, J. Cryst. Growth **44**, 513 (1978).
[11] Vergard's law has been applied for the elastic constants of $Si_{0.76}Ge_{0.24}$.
[12] S. Christiansen, M. Albrecht, H. P. Strunk, and H. J. Maier, Appl. Phys. Lett. **64**, 3617 (1994).
[13] M. Hanke, T. Boeck, A.-K. Gerlitzke, F. Syrowatka, and F. Heyroth, Phys. Rev. B **74**, 153304 (2006).
[14] N. Zakharov, P. Werner, G. Gerth, L. Schubert, L. Sokolov, and U. Gösele, J. Cryst. Growth **290**, 6 (2006).